Injection locking and synchronization in Josephson photonics devices

Lukas Danner[1,2,*] Ciprian Padurariu[2,†] Joachim Ankerhold,[2,‡] and Björn Kubala[1,2,§]

[1]*Institute of Quantum Technologies, German Aerospace Center (DLR), Söflinger Straße 100, D-89077, Ulm, Germany*
[2]*Institute for Complex Quantum Systems and IQST, Ulm University, Albert-Einstein-Allee 11, D-89069 Ulm, Germany*

Injection locking can stabilize a source of radiation, leading to an efficient suppression of noise-induced spectral broadening and therefore, to a narrow spectrum. The technique is well established in laser physics, where a phenomenological description due to Adler is usually sufficient. Recently, locking experiments were performed in Josephson photonics devices, where microwave radiation is created by inelastic Cooper pair tunneling across a dc-biased Josephson junction connected in-series with a microwave resonator. An in-depth theory of locking for such devices, accounting for the Josephson nonlinearity and the specific engineered environments, is lacking. Here, we study injection locking in a typical Josephson photonics device where the environment consists of a single mode cavity, operated in the classical regime. We show that an in-series resistance, however small, is an important ingredient in describing self-sustained Josephson oscillations and enables the locking region. We derive a dynamical equation describing locking, similar to an Adler equation, from the specific circuit equations. The effect of noise on the locked Josephson phase is described in terms of phase slips in a modified washboard potential. For weak noise, the spectral broadening is reduced exponentially with the injection signal. When this signal is provided from a second Josephson device, the two devices synchronize. In the linearized limit, we recover the Kuramoto model of synchronized oscillators. The picture of classical phase slips established here suggests a natural extension towards a theory of locking in the quantum regime.

I. INTRODUCTION

A number of experiments have demonstrated injection locking in solid-state devices that generate microwave radiation, e.g., double quantum dot masers [1] and Josephson microwave amplifiers [2]. Recently, injection locking has also been observed in a Josephson photonics device dubbed the Josephson laser [3] refining earlier experiments employing a Cooper pair transistor [4]. Josephson photonics devices use inelastic Cooper pair tunneling across a Josephson junction to convert the energy from a constant voltage bias source into microwave radiation of corresponding frequency. By applying a small amplitude ac signal on top of the dc voltage bias, a small locked region was found in Ref. [3], where the spectrum of the emitted microwave radiation becomes an extremely sharp peak pinned to the frequency of the injected signal. Injection locking may prove a key enabling technology for Josephson photonics devices and, as we will show here, also allows us to study interesting synchronization phenomena when realized by coupling different devices.

The typical setup of Josephson photonics devices consists of a voltage-biased Josephson junction coupled in series to a microwave cavity. The cavity acts as an environment engineered to absorb the energy of the tunneling Cooper pair as

microwave photons [5]. These devices have been developed as efficient sources of *quantum* microwaves by tailoring the properties of the cavity, or by deploying several cavities in series. In that manner, recent experiments have demonstrated bright single-photon sources [6,7] as well as sources of two-mode light with nonclassical correlations [8] and of entangled photons [9]. Theoretically, Josephson photonics devices have been proposed as platforms for nonlinear dynamics experiments that take advantage of the strong Josephson nonlinearity and can be operated both in the classical and in the quantum regimes [10–27] by designing low- or high-impedance resonators.

The scope of these varied applications can be significantly broadened by enhancing the phase stability of the emitted light against electronic noises, currently an outstanding challenge. While phase stability is a ubiquitous issue in microwave photonics of all types, Josephson photonics devices are particularly susceptible because the radiation is generated using a constant voltage source. This does not provide a reference phase and thus favors no particular value of the oscillation phase, i.e., in the language of nonlinear dynamics the phase is neutral.

Here, we will show that injection locking is an efficient method to achieve phase stability of Josephson photonics circuits. In this approach, an ac signal is injected directly into the circuit, with the purpose of phase locking the coupled Josephson and cavity oscillations. Furthermore, injection locking straightforwardly extends to a scenario where an ac signal stemming from one Josephson photonics circuit is used to lock another one so that the two devices synchronize. While exploring injection locking and synchronization as paradigmatic

———————
*[*]lukas.danner@uni-ulm.de
[†]ciprian.padurariu@uni-ulm.de
[‡]joachim.ankerhold@uni-ulm.de
[§]bjoern.kubala@uni-ulm.de

examples of nonlinear classical dynamics in a new system class is of interest in itself, Josephson photonics devices will allow future studies to extend such investigations to a regime where the dominant source of noise is due to quantum fluctuations. In particular, as we will later argue, injection locking in these devices could become a promising platform for studying quantum tunneling of the Josephson phase, a phenomenon analogous to the flux tunneling, or quantum phase slips [28], observed in thin superconducting wires [29–32].

The textbook theoretical description of injection locking is based on a phenomenological approach due to Adler [33]. Applied to a universal class of oscillators, termed self-sustained oscillators, the Adler equation describes their effective dynamics by a single equation for the (limit cycle) phase in the locked region and its vicinity [34]. Experimentally observed features in Ref. [3], such as frequency pulling and a scaling of the locking region's width with the amplitude of the injection signal, can successfully be described by such an approach. However, a derivation of the effective Adler equation starting from the fundamental underlying equations of motion, the Josephson circuit equations, has not been established. In consequence, the crucial parameter of the Adler model, the critical detuning that defines the locked region, has not been connected to the device properties, which in turn means that the optimal design of Josephson photonics devices for locking remains unknown.

In fact, the Josephson laser in Ref. [3] operated in a large dc-voltage bias regime, where microwaves are emitted at a down-converted frequency from a multimode cavity, and the resulting dynamics of the device is complicated and highly nonlinear. Recently, a theoretical description of the device dynamics was formulated [22], that describes the microwave emission using an approach based on a semiclassical system of coupled nonlinear differential equations. However, the model used could not capture the observed injection locking phenomena. The reason for this could not be clearly identified and to the best of our knowledge has remained an open challenge until now. The experiment Ref. [3] and the theory of Ref. [22] have been taken to imply that the highly nonlinear microwave emission generated in the Josephson laser and possibly the presence of a multimode cavity, may be a requirement for observing injection locking. As we show here, this interpretation turns out to be inaccurate, emphasizing the need for theoretical understanding of injection locking in Josephson photonics devices, particularly the theoretical description of the simplest Josephson photonics device that can be injection locked. Absent such a description, the best design, the circuit parameters, and the bounds on noises required to observe injection locking have not been systematically identified for Josephson photonics devices.

We find that adding a resistance in series with the conventional Josephson photonics device of a voltage-biased single-mode cavity is the important ingredient enabling injection locking. In fact, the in-series resistance realizes a model for an actual source, which is always somewhere in between the idealized voltage and current bias. If this resistance is small, as we will assume, the source is closer to an idealized voltage bias.
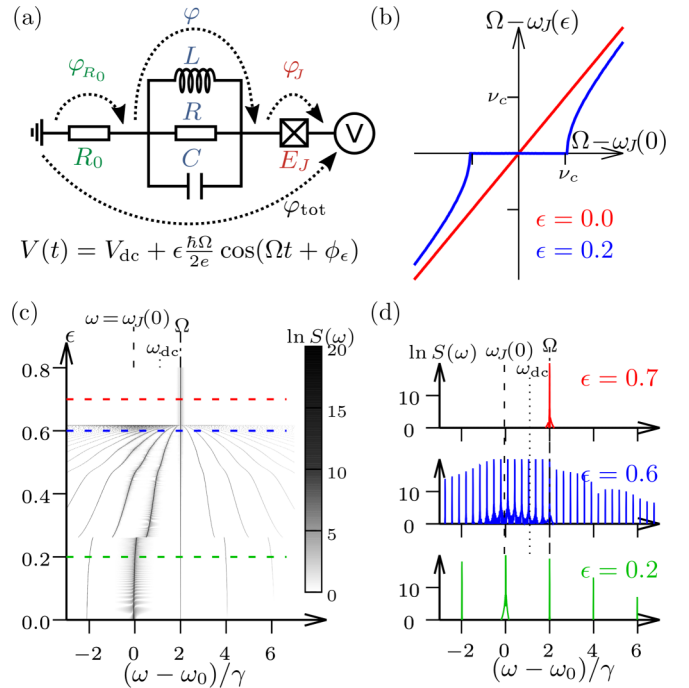

FIG. 1. Injection locking of Josephson oscillations. (a) Sketch of a Josephson photonics circuit with an in-series resistance and a single resonance (with frequency $\omega_0 = 1/\sqrt{LC}$ and width $\gamma = 1/RC$). (b) Typical Adler curve showing injection locking [$\omega_J(\epsilon) = \Omega$] as the Josephson frequency $\omega_J(\epsilon)$ is pulled towards the locking frequency Ω. Without a locking signal the Josephson frequency $\omega_J(0)$ is determined by the voltage bias, $\omega_{\mathrm{dc}} = 2eV/\hbar$, reduced by the voltage drop at the in-series resistance R_0 [$\omega_J(0) \approx \omega_0 + 2\gamma$; $\omega_{\mathrm{dc}} = \omega_0 + 2.3\gamma$]. Locking occurs for detunings, $\Omega - \omega_J(0)$, below a critical value $\nu_c(\epsilon) = \frac{e}{\hbar} I_c R_0 \epsilon$, see Sec. III. (c) Grayscale plot of emission spectrum $S(\omega, \epsilon)$ and (d) cuts for various locking signal amplitudes ϵ. In the locked state all emission occurs at the locking frequency Ω, whereas without a locking signal the cavity emits at the Josephson frequency given by the (reduced) dc bias, $\omega_J(0)$. The transition is marked by a characteristic fan structure. [Parameters values for $\omega_{\mathrm{dc}}, \omega_J(0)$ in (c) and (d) differ from (b) as indicated on the figure; other parameters: $Q = \omega_0/\gamma = 30$, $\frac{2e}{\hbar} I_c R/\omega_0 = \tilde{I}_c = 0.5$, $\frac{2e}{\hbar} I_c R_0 = v_{R_0} = \frac{4}{30}\omega_0$.]

Here, we study injection locking and synchronization in Josephson photonics devices in the classical regime. We show that injection locking can be achieved in the simplest Josephson photonics device, i.e., a device where the environment consists of an LC resonance, (a *single-mode* cavity), and a (small) in-series resistance R_0, see Fig. 1(a). We mainly focus on the case when the bias voltage is set close to this resonance, $2eV_{\mathrm{dc}}/\hbar = \omega_{\mathrm{dc}} \approx \omega_0 = 1/\sqrt{LC}$, and only briefly discuss the situation where the radiation is a result of parametric down conversion, when the bias is tuned near twice the value of the resonance frequency. For this model, we derive analytically the device-specific Adler-type equation starting from the Kirchhoff equations of the circuit. The Adler-equation allows us to explain all typical locking phenomena [see Figs. 1(b)–1(d)] resulting from the Kirchhoff equations of motion. Based on the Adler equation, we also provide bounds on the electric noises that can be stabilized, and suggestions for optimal device design.

TABLE I. Physical quantities that characterize the device.

Physical quantity	Parametrization	Unit
resonance frequency	ω_0	s^{-1}
resonance width	$\gamma = (RC)^{-1}$	s^{-1}
dc bias voltage	$\omega_{dc} = (2e/\hbar)V_{dc}$	s^{-1}
Josephson frequency	$\omega_J \neq \omega_{dc}$	s^{-1}
injection signal frequency	Ω	s^{-1}
scale of residual voltage at R_0	$v_{R_0} = (2e/\hbar)I_c R_0$	s^{-1}
Josephson driving strength	$\tilde{I}_c = (2e/\hbar)I_c R/\omega_0$	1
injection signal amplitude	$\epsilon = (2e/\hbar)V_{ac}/\Omega$	1

In Sec. II we will analyze the semiclassical nonlinear behavior of our model circuit based on the Kirchhoff equations and explain the concepts of forced versus self-sustained oscillations. In Sec. III we derive the analytical equation of Adler type that describes the injection locking region and the slow dynamics of the Josephson phase just outside the locked region. The effects of noise, the appearance of phase slips, and the reduction of the line width are presented in Sec. IV. Section V deals with locking at higher-order resonances, while in Sec. VI we turn to the synchronization of two capacitively coupled copies of the Josephson photonics device. Finally, Sec. VII presents our concluding remarks and an outlook on future work.

II. PRELIMINARIES

We study a Josephson photonics device modeled by the circuit in Fig. 1(a). The dynamics of the circuit is conveniently parametrized by the phase drop over the Josephson junction φ_J and the phase across the LC resonator φ. The classical equations of motion are the Kirchhoff equations of the circuit

$$\dot{\varphi}_J = \frac{2e}{\hbar}V(t) - \frac{2e}{\hbar}I_c R_0 \sin(\varphi_J) - \dot{\varphi}; \tag{1a}$$

$$\ddot{\varphi} + \gamma\dot{\varphi} + \omega_0^2\varphi = \frac{2eI_c R}{\hbar\omega_0}\gamma\omega_0 \sin\varphi_J. \tag{1b}$$

Here, $\omega_0 = 1/\sqrt{LC}$ is the resonance frequency and $\gamma = 1/RC$ is the resonance width. The parametrization of physical quantities characterizing the device used frequently throughout the paper is organized in Table I.

Before showing in Sec. III in detail how Eq. (1) allows the phase of the radiation emitted by the circuit to be stabilized by a locking signal, we want to gain some physical intuition, how the Josephson nonlinearity impacts the dynamics described by Eq. (1) within or outside of the locked regime.

While nonlinearity is generically known as a crucial ingredient for locking and synchronization phenomena, nonlinear effects have also been extensively studied (theoretically and experimentally) for Josephson photonics circuits, where $R_0 \equiv 0$ and locking phenomena are absent. In that case Eq. (1a) can be directly integrated [setting $\varphi_J(0) + \varphi(0) = 0$] and substituted in (1b) resulting in $\ddot{\varphi} + \gamma\dot{\varphi} + \omega_0^2\varphi = \tilde{I}_c\gamma\omega_0 \sin[\frac{2e}{\hbar}\int_0^t dt' V(t') - \varphi]$, the standard equation of motion of (classical) Josephson photonics (cf. Refs. [12]

and [17]) describing a *harmonic* LC resonator with an *unconventional nonlinear drive term*.

Considering a pure dc drive close to the fundamental resonance, $\omega_{dc} - \omega_0 \lesssim \gamma$, it is easy to see, that for small $\tilde{I}_c \ll 1$, the oscillation amplitude of $\varphi(t)$ remains small and the zeroth-order expansion of the Josephson nonlinearity in φ yields a linearly driven harmonic oscillator, that responds with an oscillation described by a complex amplitude $\tilde{\varphi}$ with $|\tilde{\varphi}| = |\tilde{I}_c\gamma/[2(\omega_{dc} - \omega_0) + i\gamma]|$.

For larger $\tilde{I}_c$ a rotating-wave approximation yields a time-independent equation for the oscillation amplitude at frequency ω_{dc} (higher harmonics of ω_{dc} are off resonant and can be neglected)

$$\tilde{\varphi} = \tilde{I}_c \frac{\gamma}{2(\omega_{dc} - \omega_0) + i\gamma}\left(J_0(|\tilde{\varphi}|)\frac{\tilde{\varphi}^*}{|\tilde{\varphi}|} - J_2(|\tilde{\varphi}|)\frac{\tilde{\varphi}}{|\tilde{\varphi}|}\right).$$

The Bessel functions of the first kind are manifestations of the highly nonlinear Josephson drive and can give rise to bifurcations and multistable states in this regime.

Adding a small ac signal to the voltage drive,

$$V(t) = V_{dc} + V_{ac}\cos(\Omega t + \phi_\epsilon), \tag{2}$$

leads to a simple superposition of responses with the two frequencies ω_{dc} and Ω, if R_0 is neglected.

In most of the following, to emphasize the simplest locking scheme, we restrict our study to locking of the linear regime of Josephson photonics, where $\tilde{I}_c \ll 1$. Despite the small amplitude of resonant oscillations in this regime, it is the presence of the in-series resistance R_0, which will lead to a different manifestation of Josephson nonlinearity and pave the path to locking and synchronization phenomena. To understand the nature of this distinct nonlinear effect, we have to consider how the presence of a finite resistance R_0 modifies the picture of the driven oscillator sketched above.

Origin of locking. For finite but small $R_0 \ll R$, and $\tilde{I}_c \ll 1$ so that φ remains small, Eq. (1a) can be iteratively integrated

$$\varphi_J(t) = \int_0^t dt'\left\{\frac{2e}{\hbar}V(t') - v_{R_0}\sin[\varphi_J(t')]\right\} - \varphi(t)$$

$$\approx \frac{2e}{\hbar}\int_0^t dt' V(t') - \varphi(t)$$

$$- v_{R_0}\int_0^t dt_1 \sin\left[\frac{2e}{\hbar}\int_0^{t_1} dt_2 V(t_2)\right] \tag{3}$$

in a Born-like approximation up to leading order in the small quantities $\tilde{I}_c$ and (v_{R_0}/ω_0). (Note also that φ is small with $|\tilde{\varphi}| \propto \tilde{I}_c$.)

In addition to the dc and ac components of the voltage drive, the presence of R_0 gives rise to a low-frequency Fourier component $\tilde{\varphi}_J(\nu) = \mathcal{F}[\varphi_J(t)]_\nu$, at the frequency of beats $\nu = (\omega_{dc} - \Omega)$ caused by a slowly oscillating part of the Josephson current $I_J \sim \sin\varphi_J$. In fact, we find

$$|\tilde{\varphi}_J(\nu)| = v_{R_0}\mathcal{F}\left[\int_0^t dt_1 \sin\left(\frac{2e}{\hbar}\int_0^{t_1} dt_2 V(t_2)\right)\right]_\nu$$

$$= \frac{\epsilon}{2}\frac{v_{R_0}}{\nu},$$

i.e., *the closer the frequencies of locking signal Ω and dc drive ω_{dc} become, the slower the oscillations in I_J, and the larger the integrated effect in the $\tilde{\varphi}_J(\nu)$ oscillations.*

In consequence, even for small locking amplitude ϵ and small, but finite, v_{R_0} the low-frequency oscillations in the Josephson phase $\tilde{\varphi}_J(\nu)$ can become so large that (despite $\tilde{I}_c \ll 1$) the nonlinearity of the driving term $\sim \sin \varphi_J$ in Eq. (1b) comes to bear. This nonlinearity of the slow response produces an increasing number of sidebands in the oscillator response $\tilde{\varphi}$ around the Josephson frequency, each sideband separated by ν, as seen in Fig. 1(d), until eventually the oscillations lock, with the response concentrated at frequency Ω, cf. the typical fan structure of Fig. 1(c).

While in Sec. III, we will properly derive the corresponding locked and unlocked solution, from the simple arguments above one can already estimate the locking range; namely by the onset of the new type of nonlinearity as $1 \overset{!}{=} |\tilde{\varphi}_J(\nu)| = (\epsilon/2)(v_{R_0}/\nu)$, which yields a locking region

$$|\nu| = |\Omega - \omega_{\mathrm{dc}}| \leqslant \nu_c = \tfrac{1}{2}\epsilon v_{R_0}. \qquad (4)$$

Considering the crucial role any residual in-series resistance R_0 plays in establishing the nonlinear locking dynamics, it may seem surprising that it was mostly neglected in previous studies of Josephson photonics. This is justified by the observation that without an ac signal the residual resistance merely leads to a small and constant shift of the dc voltage with no significant consequence for the dynamics.[1] Only in combination with an additional injection signal, the residual resistance becomes a key parameter enabling low-frequency oscillations to access the nonlinear regime. The shift of the dc voltage, $I_{\mathrm{dc}} R_0$, becomes dependent on this nonlinear response $\varphi(t)$, so that the effective dc voltage seen by the junction and the resulting Josephson frequency is pulled and the Josephson oscillations can lock to the ac signal.

Forced and self-sustained oscillations. In the language of nonlinear dynamics, without R_0 the Josephson junction undergoes *forced oscillations*, where the Josephson frequency is directly fixed to the dc bias. The forced oscillations respond linearly to an injection signal. At finite R_0, the Josephson frequency becomes a dynamical quantity, different from the dc bias, which is determined by the equation

$$\omega_J = \omega_{\mathrm{dc}} - \frac{2e}{\hbar} I_{\mathrm{dc}}[\varphi; \varphi_J] R_0, \qquad (5)$$

where the dc part of the Josephson current, I_{dc}, depends on the solutions $\{\varphi(t), \varphi_J(t)\}$. In this case, the Josephson oscillations are *self-sustained oscillations* and can be locked.

These properties of a Josephson photonics device with an in-series resistance are demonstrated in Fig. 2. The cavity degree of freedom φ is driven to oscillations with $\omega_J < \omega_{\mathrm{dc}}$ according to (5). In the weak driving regime, $\tilde{I}_c \ll 1$, these are purely sinusoidal and correspond to a single point in Fig. 2(a)
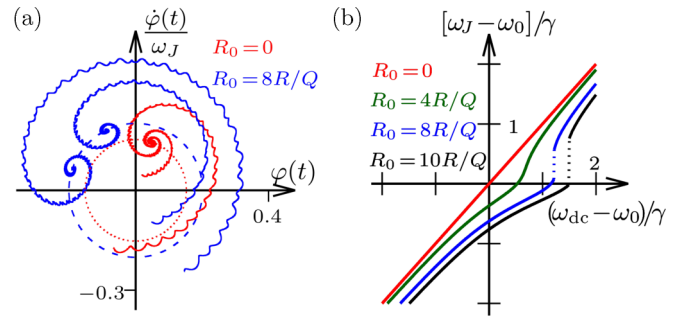

FIG. 2. Properties of Josephson oscillations without a locking signal. (a) Phase-space picture (in the frame rotating with ω_J) of the cavity dynamics showing trajectories (solid) relaxing towards limit cycles (dashed). Without in-series resistance a Josephson photonics circuit is forced into oscillations with a fixed, stable phase, so that all perturbations relax back to the same phase-space (fixed) point (red, dots: laboratory frame). The additional degree of freedom provided by an in-series resistance allows different perturbations to relax to different points along the limit cycle (blue). This freedom of the phase on the limit cycle makes a self-sustained oscillator susceptible to locking. Note that, in the reduced phase space of the cavity, trajectories may cross. (b) The oscillation frequency of the cavity, $\omega_J(0)$, is reduced from the dc bias, $\sim \omega_{\mathrm{dc}}$, by the (dc) voltage drop at the in-series resistance. For small R_0, this reduction is given by the Lorentzian resonance curve of Josephson photonics (red vs. green curve), whereas at larger R_0 an instability occurs [cf. the discontinuity in Fig. 1(c) at $\epsilon \approx 0.26$]. [Parameters: $\omega_{\mathrm{dc}} = \omega_0 + 1.5\gamma$, $0 \leqslant \omega_0 t \leqslant 450$ in (a); for other parameters see Fig. 1 and legends.]

in a frame rotating with ω_J. Depending on initial conditions different angles on a circular limit cycle are found in the long-time limit. Perturbations from this (nonequilibrium) steady state relax to a (possibly different) point on the limit cycle. These are all the typical features of a self-sustained oscillator, such as the van der Pol oscillator, with the slightly more complex relaxation dynamics here being caused by the extra degree of freedom φ_J. In contrast, without R_0, oscillations occur with $\omega_J \equiv \omega_{\mathrm{dc}}$ and a fixed phase angle (only depending on the choice of the rotating frame)[2] that corresponds to a single point on a cycle, stable against perturbations.

Figure 2(b) visualizes how the in-series resistance R_0 impacts the frequency of Josephson oscillations even in the absence of a locking signal. Without R_0 the Josephson frequency is given by the dc bias ($\omega_J = \omega_{\mathrm{dc}}$, red), whereas as described by Eq. (5) for finite R_0 it is reduced by the (average) voltage drop at the in-series resistance R_0 due to the dc part of the Josephson current I_{dc}. For small R_0 (green) this reduction is simply given by the standard resonance curve of Josephson photonics, where I_{dc} (and the photon emission) peaks at the fundamental cavity resonance $\omega_{\mathrm{dc}} = \omega_0$ with a resonance width determined by the cavity decay rate γ. Increasing R_0 (blue, black) the resonance is shifted to larger ω_{dc} compensating for the portion of the voltage dropping at R_0. For voltages above the resonance peak, i.e., at the flank

---

[1]It has been noted, however, that a model without R_0 and a strictly fixed dc bias would result in emission without spectral width, and the observed spectral linewidth, typically much sharper than the inverse cavity lifetime, has been associated with low-frequency fluctuations of the voltage at the junction

---

[2]Note that there is a subtlety in defining the phase of the rotating frame and there is also a valid approach which results in a limit cycle description for the $R_0 = 0$ case, but does not lead to locking.

of the resonance curve where $Y_J = (2e/\hbar)\partial I_{dc}/\partial\omega_J < 0$, an instability develops, once $Y_J \leqslant -1/R_0$, so that the total device admittance vanishes. Formally, this follows by differentiating Eq. (5) with respect to ω_J, where $\partial\omega_{dc}/\partial\omega_J = 0$ corresponds to the jumps in Fig. 2(b).

III. INJECTION LOCKING

In this section, we derive explicit equations describing the nonlinear behavior developing at small detuning $\nu \simeq \nu_c \ll \omega_J, \Omega$ and show that it results in frequency pulling and locking. In particular, we derive the equations governing the dynamics of the circuit at the slow frequency ν and show the similarity to the Adler equation, a universal equation describing injection locking in self-sustained oscillators.

Slow dynamics will describe how the circuit response shifts from oscillations at the natural frequency of the self-sustained oscillator ω_J to the frequency Ω of the locking signal. The definition of ω_J by Eq. (5) applies in the presence of a locking signal, so that $\omega_J = \omega_J(\epsilon)$ with $\omega_J(\epsilon) \equiv \Omega$ when the oscillations are locked.

In the limit of weak Josephson coupling $\tilde{I}_c \ll 1$ and small residual resistance $R_0 \ll R$, we can neglect the components of φ_J oscillating at multiples of the Josephson frequency. However, for a small frequency ν when phase locking develops, we must account for sidebands around ω_J at multiples of ν. We express these sidebands by slowly varying parameters in an ansatz for junction and cavity phases. Since locking primarily relies on the adaption of frequencies and phases, we

can justifiably neglect a slow time dependence of oscillation amplitudes and write

$$\varphi_J(t) = \omega_J t + \theta_J(t) + a_J \sin[\omega_J t + \phi_J(t)] \tag{6}$$

to capture the driven dynamics of the junction phase consistent with our considerations above, cf. Eq. (3). For the cavity phase we similarly chose the ansatz,

$$\varphi(t) = a \sin[\omega_J t + \phi(t)], \tag{7}$$

which neglects the off-resonant response of the cavity phase, assuming a large quality factor, $Q \gg 1$, as is typical in Josephson photonics devices.

Time-scale separation. All unknown functions, $\theta_J(t)$, $\phi_J(t)$ and $\phi(t)$, are slowly varying in time, with $\dot\theta_J$, $\dot\phi_J$, $\dot\phi \simeq \nu \ll \omega_J$, while the fast frequencies are only slightly detuned from each other, $\omega_J \simeq \omega_{dc} \simeq \omega_0$. We can thus use time-scale separation for the two time scales $\omega_J^{-1} \ll \nu^{-1}$ to obtain equations for the slowly varying functions. Inserting the ansatz in the circuit equations Eqs. (1a) and (1b), we can separate each resulting equation in a slow part and a part containing fast oscillations. The relation

$$\dot\theta_J = (\omega_{dc} - \omega_J) - \nu_{R_0}\frac{a_J}{2}\sin(\phi_J - \theta_J), \tag{8}$$

follows from the low-frequency terms of Eq. (1a), while the corresponding result from Eq. (1b) yields an irrelevant offset of the ϕ oscillations.

Isolating terms with frequencies close to ω_J in Eq. (1a) and Eq. (1b), respectively, yields

$$\omega_J a_J \cos(\omega_J t + \phi_J) = \epsilon\Omega\cos(\Omega t + \phi_\epsilon) - \nu_{R_0}\sin(\omega_J t + \theta_J) - a\omega_J\cos(\omega_J t + \phi), \tag{9a}$$

$$\tilde{I}_c\omega_0\gamma\sin(\omega_J t + \theta_J) = a\{[\omega_0^2 - (\omega_J + \dot\phi)^2]\sin(\omega_J t + \phi) + \gamma\omega_J\cos(\omega_J t + \phi)\}. \tag{9b}$$

Equations (9a) and (9b) can be rewritten in a frame rotating with frequency ω_J, where they are equivalent to the following set of complex equations,

$$a_J e^{i\phi_J} = \epsilon e^{i\phi_\epsilon}e^{i(\Omega - \omega_J)t} + i\frac{\nu_{R_0}}{\Omega}e^{i\theta_J} - ae^{i\phi}, \tag{10a}$$

$$ae^{i\phi} = \tilde{I}_c\frac{\gamma}{[2(\omega_0 - \omega_J - \dot\phi) + i\gamma]}e^{i\theta_J}. \tag{10b}$$

Equations (10a) and (10b), together with Eq. (8), form a set of five real-valued algebraic equations that can be solved for three unknown real-valued slowly varying functions θ_J, ϕ_J, and ϕ, and two real-valued parameters a_J and a.

Deriving an Adler equation. The injection locking phenomenon emerges by solving the above system of equations. However, the full analytical solution is cumbersome and fortunately, its behavior can be discussed quantitatively using a simplification commonly used in nonlinear sciences. The simplification arises when the system of equations is reduced to a single Adler-type equation, where a locking region can be directly identified. To derive the Adler-type equation analytically, we proceed by substituting Eq. (10b) into Eq. (10a), then taking the imaginary part of Eq. (10a) to obtain an expression for $a_J \sin(\phi_J - \theta_J)$. Finally, the latter expression can

be substituted into Eq. (8) to arrive at

$$\dot\theta_J = (\omega_{dc} - \omega_J) - \frac{\nu_{R_0}}{2}\Bigg[\epsilon\sin\left[(\Omega - \omega_J)t - \theta_J + \phi_\epsilon\right]$$
$$+ \frac{\nu_{R_0}}{\Omega} + \tilde{I}_c\frac{\gamma^2}{4(\omega_0 - \omega_J - \dot\phi)^2 + \gamma^2}\Bigg]. \tag{11}$$

Equation (11) captures the dynamics of the circuit at the slow time scale ν^{-1}, describing the nonlinear response of the circuit to the injection signal. The analogy to the Adler equation becomes evident by defining the phase shift between slow components of the Josephson phase and the injection signal,

$$\psi(t) = \omega_J t + \theta_J - \Omega t - \phi_\epsilon. \tag{12}$$

In the phase-locked regime, where $\theta_J = \text{const.}$ and $\omega_J = \Omega$, the phase $\psi(t)$ becomes constant in time, $\dot\psi = 0$. Substituting the expression of ψ into Eq. (11) we arrive at

$$\dot\psi = \nu(\epsilon, \Omega) - \nu_{R_0}\frac{\epsilon}{2}\sin(\psi), \tag{13}$$

with the detuning $\nu(\epsilon, \Omega)$ defined as

$$\nu(\epsilon, \Omega) \equiv \nu_0(\Omega) + \Delta\nu(\epsilon, \Omega), \tag{14}$$

where ν_0 is the detuning between the injection frequency Ω and the Josephson frequency at $\epsilon = 0$, i.e., before the injection

signal is applied, and $\Delta \nu(\epsilon, \Omega)$ is the self-consistent change in the Josephson frequency, owing to the frequency dependence

of the cavity response. These two terms have the following expressions:

$$\nu_0(\Omega) = \left(\omega_{\mathrm{dc}} - \frac{v_{R_0}}{\Omega} \frac{v_{R_0}}{2} - \frac{\tilde{I}_c}{2} \frac{\gamma^2}{4[\omega_0 - \omega_J(0)]^2 + \gamma^2} v_{R_0} \right) - \Omega. \tag{15}$$

$$\Delta \nu(\epsilon, \Omega) = \frac{\tilde{I}_c}{2} \left[\frac{\gamma^2}{4[\omega_0 - \omega_J(0)]^2 + \gamma^2} - \frac{\gamma^2}{4[\omega_0 - \omega_J(\epsilon, \Omega) - \dot{\phi}(\epsilon, \Omega)]^2 + \gamma^2} \right] v_{R_0}. \tag{16}$$

The detuning ν that depends on both the injection amplitude ϵ as well as frequency Ω, together with the prefactor of the sine term $(\epsilon/2)v_{R_0}$, reflect an Adler-type equation that is specific to Josephson photonics circuits. This is a central result of this paper.

Arnold tongues as locked regions. The Adler equation, Eq. (13), reveals the phase-locked region marked by solutions where $\dot{\psi}(t) = 0$. Such solutions exist for any fixed injection signal amplitude ϵ, as long as the injection frequency Ω is tuned such that $|\nu(\epsilon, \Omega)| < (\epsilon/2)v_{R_0}$. In that case, we find the time-independent solution ψ given by,

$$\psi = \arcsin \left(\frac{2\nu(\epsilon, \Omega)}{\epsilon v_{R_0}} \right) \pmod{2\pi}. \tag{17}$$

The edges of the phase-locked region are determined by the self-consistent equation,

$$|\nu(\epsilon, \Omega)| = \frac{1}{2} \epsilon v_{R_0}. \tag{18}$$

The resulting phase-locked region typically increases as a function of ϵ, creating a shape termed the Arnold tongue. In Fig. 3 we show such Arnold tongues, first in the case when the dc bias is chosen such that the Josephson frequency in the absence of injection signal is near the resonance of the cavity, $\omega_J(0) \approx \omega_0$, and second, in the case when the frequencies are far from the cavity resonance frequency.

Away from the resonance, in the frequency range where the electromagnetic environment of the junction is featureless, the term $\Delta \nu(\epsilon)$ is suppressed and can be neglected if $R \ll R_0$. In this limit, the cavity can be neglected and the circuit becomes equivalent to a resistively shunted Josephson junction (RSJ). For the RSJ model, Eq. (13) takes the canonical form of the Adler equation,

$$\dot{\psi} = \nu_0 - v_{R_0} \frac{\epsilon}{2} \sin(\psi). \tag{19}$$

For a sufficiently strong drive and small detuning ν_0, such that $\nu_0 \leqslant \nu_c$ with $\nu_c \equiv v_{R_0}(\epsilon/2)$, the Adler equation admits a time-independent solution $\psi_0 = \arcsin(\nu/\nu_c)$ that describes locked oscillations, $\dot{\varphi}_J = \Omega$, [see Fig. 1(b)] with relative phase ψ_0. For the RSJ model, the phase-locked region describes the well-known Shapiro step [35], occurring at $2e\langle V_J \rangle = \hbar\Omega$ between current plateaus in the I(V) curve. Linearization in the Josephson driving strength is of course not necessary in this far off-resonant regime, which has been extensively described in the past using a variety of theoretical methods in the context of the Josephson voltage standard [36], a mature field that we do not review here.

Alternatively to an oscillatory voltage, injection locking can also be achieved by injecting an ac current directly into

the cavity of the Josephson device. The properties of locking are qualitatively similar to those described in this section. For completeness and due to the possible relevance for future experimental implementations, we have described in detail the derivation of the effective Adler equation for direct ac-current locking in the Supplemental Material [37].

Washboard potentials and locking signatures. It may be helpful to emphasize at this point the difference between two washboardlike potentials for the dynamics of different phase-like variables, which appear in the locking scenario. First, the washboard potential for the dynamics of the Josephson phase φ_J, obtained by Eq. (1a), describes a potential with a periodic part given by the Josephson coupling, and a tilt, which oscillates in time with an amplitude proportional to ϵ around an average value set by the dc voltage (with an additional term describing the coupling to the cavity variable).
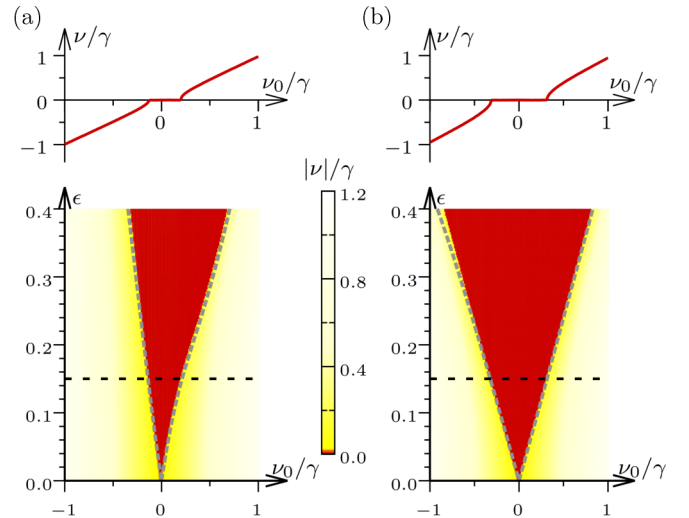

FIG. 3. Arnold tongues. In the locked region (red area in bottom panels and $\nu \equiv 0$ in top panels) the Josephson frequency, $\omega_J(\epsilon)$ becomes equal to the locking frequency, $\nu = \omega_J - \Omega \equiv 0$. The initial ($\epsilon = 0$) detuning, $\nu_0 = \omega_J(0) - \Omega$, is varied by changing the locking frequency Ω for a constant dc bias. (a) If the initial Josephson frequency is close to the cavity resonance [$\omega_J(0) \approx \omega_0 - \gamma/20$ found for $\omega_{\mathrm{dc}} = \omega_0 + 0.39\gamma$] the Arnold tongue is strongly deformed for $\epsilon \lll 1$, while (b) for off-resonant biasing [$\omega_J(0) \approx \omega_0 + 2\gamma$ found for $\omega_{\mathrm{dc}} = \omega_0 + 2.3\gamma$] the standard linear Arnold tongue shape is recovered. Black dashed lines indicate the position of the horizontal cuts shown in the top panels. Gray dashes are the analytical results for the locking boundaries based on the derived effective Adler equation, Eqs. (13)–(16). [The Josephson driving strength is (a) $\tilde{I}_c = 0.3$ and (b) $\tilde{I}_c = 0.5$. Other parameters are the same as in Fig. 1.]

Without ac drive and cavity, this is, of course, just the familiar RSJ potential for an overdamped junction describing, e.g., transitions between a running-voltage state and the trapped state. Second, the Adler-like potential, Eq. (13), also of washboard type, associated to the dynamics of the Adler variable ψ. This potential can essentially be related to the one for φ_J by a rotating-frame description (with rotation frequency Ω), where the tilt becomes static and is reduced to the detuning, and the periodic part stems from a combination of locking signal and Josephson coupling.

While the details of Eqs. (13)–(16) and the way locking affects the cavity emission are unique to the Josephson-photonics setup, many aspects of the dynamics in the tilted washboard potential are generic: The dynamics of a particle with negligible mass in a washboard potential $U(\psi) = \nu\psi + \nu_c \cos(\psi)$ depends on the relation between tilt and oscillation amplitude. The condition $\nu \lesssim \nu_c$ corresponds to the appearance of local minima in the potential that trap the relative phase ψ and stabilize it. Just outside the locking region, $\nu \gtrsim \nu_c$, $U(\psi)$ has the shape of a staircase. The phase particle advances slowly along the flat region of the staircase, then drops rapidly along the steep region, giving rise to periodic dynamics (for ψ modulo 2π). We define the distance from the locking region, $\delta = (\nu - \nu_c)/\nu_c$ and assume $\delta \ll 1$. The time spent by the phase particle on the flat region of the staircase is given by $T_s \sim (2\pi/\nu_c)(1/\sqrt{\delta})$ and diverges as the locking region is approached, $\delta \to 0$. The rapid drop along the steep region is relatively short, $(2\pi/\nu_c)$, and can be neglected in comparison to T_s close to the locking region. The slow rise during T_s followed by a rapid drop is well described by a sawtooth function. Its period is given by the slow time scale T_s and can be represented as a Fourier series in harmonics of $\tilde{\nu} \simeq (2\pi/T_s) \sim \nu_c\sqrt{\delta}$,

$$[\psi(t) - \psi(0)]_{(\text{mod } 2\pi)} \sim \sqrt{\delta} \sum_{k=1}^{1/\sqrt{\delta}} (-1)^{k+1} \frac{\sin(k\tilde{\nu}t)}{k}, \quad (20)$$

valid close to the locking region, in the asymptotic limit $\delta \to 0$. The emergence of many, closely spaced harmonics $k\tilde{\nu}$ with $\tilde{\nu} \sim \sqrt{\delta}$ and $k = 1 \ldots 1/\sqrt{\delta}$ for $\delta \to 0$ in the dynamics of the rotating-frame variable ψ results in the fanlike spectrum of the cavity emission centered around ω_J observable in Figs. 1(c), 1(d) a telltale signature of the approach to the locking transition.

IV. EFFECTS OF NOISE

The hallmark of the injection locking phenomenon is that it stabilizes the phase of oscillations, ψ, against perturbations due to noise. To explicitly demonstrate and study this stabilization in numerical simulations stochastic noise forces are added to the equations governing the system's dynamics.

In recent Josephson photonics experiments the dominant source of noise were fluctuations $\Delta V(t)$ of the applied bias voltage, which were slow and of classical nature, and ascribed to thermal or external noises. Another unavoidable source of fluctuations is voltage noise created at the in-series resistance R_0 by the shot noise of the Josephson current across the tunnel junction. This quantum noise, stemming from the granular nature of charges, can only imperfectly be captured by a

stochastic force term in a classical equation of motion, as we will briefly discuss further below.

Following the typical experimental situation, we include Gaussian colored noise as an addition to the voltage term in Eqs. (1). Before turning again to the effective Adler equation for analytical considerations and estimates, let us discuss the effects of adding noise to Eqs. (1), as observed in the full numerical solutions. Figure 4(a) reproduces the hallmark experimental signature of locking from such solutions: the emergence of an extremely sharp peak arising from the (thermally) broadened spectrum of the cavity emission as the system enters the locking region. The same physics is described by the phase-space distributions displayed in Figs. 4(b)–4(d). Without a locking signal, weak and slow fluctuations allow the quadratures of the cavity oscillation to diffuse around the complete limit cycle (with slight excursions in radial direction). A locking signal strongly restrains this diffusion and in the rotating-frame phase space both angle and radius are stabilized in the locked regime, see Fig. 4(d).

To understand and analyze the effects of noise observed in the results of the full numerical solutions of Eqs. (1) shown in Fig. 4, we can reconsider the derivation of the effective Adler equation, now in the presence of a fluctuating noise term. Reasoning that the high-frequency components of noise fluctuations are efficiently filtered and do not reach the device, as is typically the case in Josephson photonics experiments, which corresponds to assuming a correlation time of the colored noise larger than typical time scales of the dynamics, the time-scale separation used in the previous section will remain valid in the presence of noise. It is then easy to show that noise introduces in the circuit Adler equation a stochastic frequency detuning due to the variation of the dc bias, $\xi(t) = (2e/\hbar)\Delta V(t)$,

$$\dot{\psi} = \nu(\epsilon) - \nu_{R_0} \frac{\epsilon}{2} \sin(\psi) + \xi(t) = \frac{\partial U(\psi)}{\partial \psi} + \xi(t). \quad (21)$$

To the overdamped dynamics of the phase particle in the washboard potential $U(\psi) = \nu\psi + \nu_c \cos(\psi)$ tilted by the detuning ν and with a modulation amplitude increasing with the locking strength, there now contributes a fluctuating noise force, which can alternatively be seen as a fluctuation of the tilt.

In the absence of an injection signal, the potential is a flat tilted landscape, $U(\psi, \epsilon = 0) = \nu_0\psi$; the resultant uniform motion for Ψ with velocity ν_0 corresponds to cavity emission at ω_J. In a phase space rotating with the same frequency ω_J this motion is represented by a fixed point. Noise adds (free) diffusion to the motion of the phase particle, which yields the wide spectrum for the cavity emission shown by the blue line of Fig. 4(a) and the typical donut shape in the rotating phase space, Fig. 4(b). Adding the injection signal provides a series of minima to the potential, separated by 2π, which can reduce the effects of noise, restrict the diffusion, and decrease the average velocity. In a frame rotating with this average velocity [top panel of Fig. 4(c)] one nonetheless obtains diffusion exploring the whole limit cycle and a donut-shaped phase-space distribution. The modulation of this diffusion by the injection signal only becomes apparent in a frame rotating with Ω [bottom panel of Fig. 4(c)], where a modulated donut with more or less weight indicating potential minimum and maximum is
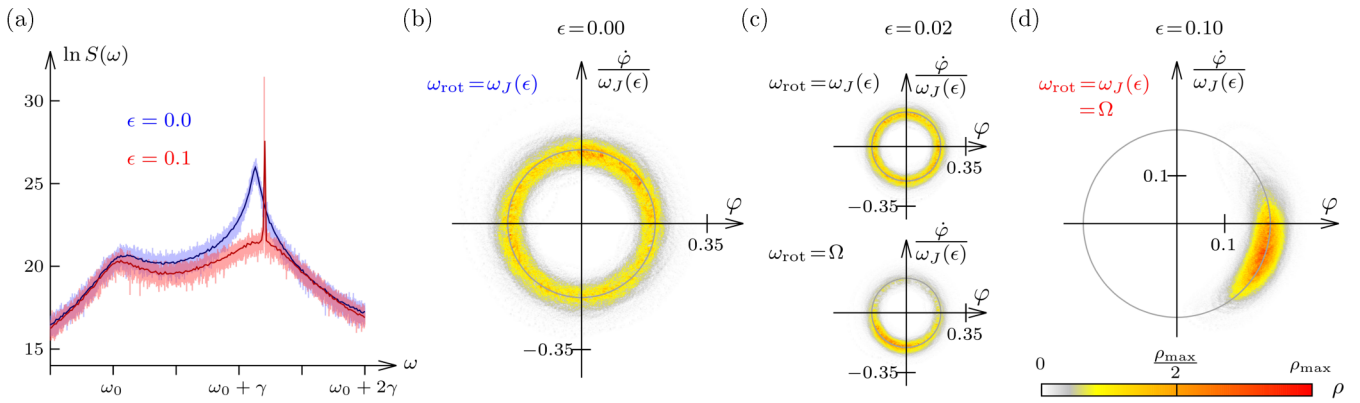
FIG. 4. Signatures of locking in classical dynamics with noise. (a) The hallmark signature of locking in the emission spectrum is the emergence of an extremely sharp peak (red) at the locking frequency Ω as compared to the unlocked (thermally) broadened emission (blue) around $\omega_J(0)$ [$\Omega = \omega_0 + 1.2\gamma$; $\omega_J(0) \approx \omega_0 + 1.13\gamma$, reduced from the dc bias, $\omega_{dc} = \omega_0 + 1.5\gamma$ due to the in-series resistance]. The cavity resonance enhances thermal fluctuations around ω_0. [Light colors show the spectrum averaged over 10 long runs with $0 \leqslant \omega_0 t \leqslant 10^6$, which is further smoothened to a resolution $\delta\omega \approx \gamma/80$ to give the solid lines. Noise is modeled by an Ornstein-Uhlenbeck process with (zero-frequency) spectral noise density, $S_\xi = \gamma/30$, and correlation time $t_{corr} = 2/\gamma$.] Phase-space distributions ρ are shown: (b) without a locking signal in a frame rotating with $\omega_J \neq \Omega$; (c) in the unlocked region for frames rotating with ω_J and with Ω; and (d) for the locked case rotating with $\omega_J = \Omega$. Diffusion around the limit cycle caused by the noise is modulated and eventually confined by increasing the locking signal. In the latter case, long-time phase correlations result in a pronounced reduction of the linewidth shown in (a). [For parameters not otherwise stated, see Fig. 1; (pseudo-)steady-state distributions are gained from a single run with $5 \times 10^5 \leqslant \omega_0 t \leqslant 10^6$.]

found. In the locked region, the distribution finally becomes strongly confined, see Fig. 4(d).

Starting from the known tilted washboard dynamics in the absence of noise, we see that adding even weak noise may have strong effects close to the onset of locking around the critical tilt ν_c. Just above the onset the average velocity of the phase particle $\omega_J - \Omega$ is approaching zero due to the slow creeping motion along the nearly flat part of the washboard. Clearly fluctuations of the tilt will cut this creeping motion short and strongly increase the average velocity, as is indeed seen in Fig. 5(c). The situation is very different deep inside the locking region, $|\nu/\nu_c| \ll 1$, where, if the spectral density of noise is smaller than the barrier height between consecutive minima, the dynamics of the locked phase particle can be qualitatively described as localized explorations of the local minimum (intrawell dynamics) combined with occasional escape events (interwell dynamics) where the phase crosses the barrier and is subsequently retrapped at the next potential minimum. These escape events are noise-assisted phase slips where the phase rapidly changes by 2π. Figures 5(a), 5(b) depicts the typical time dependence of $\psi(t)$ in the locked region and under the influence of colored noise generated by an Ornstein-Uhlenbeck process with a correlation time chosen as $2/\gamma$. The average rate of phase slips sets the average velocity $\omega_J - \Omega$, leading to deviations from the constant part of the locking curve in Fig. 5(c). The noisy dynamics of the Josephson phase particle ψ, described here on the basis of the Adler-like effective equation, is similar to known Shapiro-steps physics, where, however, there are no direct equivalents to the signatures in the cavity spectrum and the phase-space features.

In the emerging picture of locking in the presence of noise, the concept of injection locking can no longer be equivalent to $\dot{\psi} = 0$ and must be amended to account for the fact that the

relative phase ψ between the injection signal and the oscillations in the Josephson device is no longer time independent.

Instead, the stabilization of the phase will be quantified by the rate of phase slips. For a simple quantitative estimate we turn to the Kramers regime of diffusion over a barrier for overdamped dynamics [38]. Neglecting correlations between consecutive slips and for a noise spectral density $S_\xi \equiv \int d\tau \, \xi(\tau)\xi(0)$ small compared to the barrier height, U_B, the rate of phase slips Γ_{ps} is exponentially suppressed,

$$\Gamma_{ps}(U_B, S_\xi) \sim \exp\left(-\frac{U_B}{S_\xi}\right), \quad \text{for } U_B \gg S_\xi. \quad (22)$$

The barrier height has a maximum, when the detuning in the Adler equation vanishes $\nu(\epsilon) = 0$, and where locking is most stable against noise. Its maximal height can be estimated as $U_{B,max} = \nu_c \simeq eI_c R_0 \epsilon/\hbar$. This sets an upper limit for the noise intensity that can be overcome and stabilized by an injection signal with fixed amplitude ϵ,

$$S_\xi < (\epsilon/2)\nu_{R_0}. \quad (23)$$

The phase stabilization has important consequences for the spectral width of the radiation emitted by the Josephson photonics device. In absence of an injection signal, the spectral width $\delta\omega$ in the simplest linear scenario is directly set by the noise spectral density, $\delta\omega \simeq S_\xi$. By injection locking the device and tuning the injection frequency to the condition of maximum barrier height, $\nu(\epsilon) = 0$, the new spectral width will be given by the rate of phase slips, $\delta\omega \simeq \Gamma_{ps}$. This will amount to an *exponential reduction of the spectral width*, yielding an extremely sharp spectral feature when the noise intensity falls well below the above threshold, as in Fig. 4(a).

Experimental requirements. The requirements to observe the exponential reduction of the spectral width can be
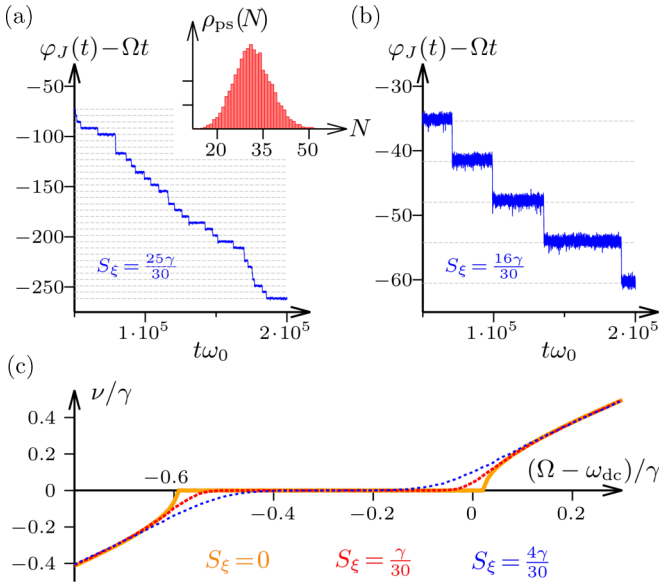
FIG. 5. Effect of noise on the dynamics of the junction phase. Noise induced diffusion allows the slow phase variable, $\varphi_J(t) - \Omega t$, to overcome the potential barrier in the tilted washboard potential described by Eq. (21) and slip by 2π from one potential minimum to the next. An increased noise strength [(a) as compared to (b)] results in a strongly (exponentially) enhanced rate of slips, Γ_{ps}, see Eq. (22). In the simplest regime, slips follow a Poissonian distribution [see histogram of 10^4 traces in inset of (a)]. The slip rate, $\Gamma_{ps} := \frac{\langle N \rangle}{\Delta t} = \frac{\langle\langle N \rangle\rangle}{\Delta t} \approx \frac{30}{1.5 \, 10^5} \omega_0$ determines the noise induced shift and linewidth of the spectral peak. [Parameters as in Fig. 2(a), $t_{corr} = 2/\gamma$]. (c) Bifurcations appearing in locking curves without noise are progressively washed out for increasing noise strength, and even deep in the locked region the average Josephson frequency differs from the locking frequency, $\omega_J(\epsilon) - \Omega \neq 0$, due to (thermal) phase slips. [Parameters cf. Fig. 3(b) top].

estimated quantitatively based on typical realizations of the Josephson photonics device in experiments [5,7–9]. For a device with small Josephson coupling $\tilde{I}_c = 2eI_cR/\hbar\omega_0 = 0.5$, as can be routinely realized, and a resonance quality factor $Z(\omega = \omega_0)/Z(\omega = 0) \approx R/R_0 \simeq 30$ (a low estimate), the barrier height that can be created with an injection signal of amplitude ϵ can be estimated to $U_{B,max} \simeq (\epsilon/2)v_{R_0} = eI_cR_0\epsilon/\hbar \simeq (\epsilon/120)\omega_0$. Furthermore, the spectral width for such a device in absence of an injection signal is typically of the order $\delta\omega \simeq 10^{-3}\omega_0$, resulting in the same estimation for the noise spectral density $S_\xi \simeq 10^{-3}\omega_0$. Therefore, the requirement to observe the exponential suppression of noise $U_{B,max} > S_\xi$ amounts to $\epsilon > 0.12$. This places the amplitude of the injection signal reasonably well in the linear regime, see Fig. 3.

In the opposite limit, when the injection amplitude is weak, such that the noise satisfies $S_\xi > (\epsilon/2)v_{R_0}$, the stabilization is negligible [the evolution of the phase $\psi(t)$ in this case is shown in Fig. 5(a)]. While in this regime the phase is not stabilized and the spectrum remains broad, injection locking may have measurable consequences in other observables, such as in the statistics of the radiation emitted by the device. Interesting questions, such as the relation between the statistics of

phase slips and the statistics of the emitted radiation, will be addressed elsewhere.

While the estimations above suggest that it may be optimal for locking to increase the resistor R_0, this step may become counterproductive if current fluctuations at R_0 become the dominant source of voltage noise. In that case, thermal noise can become negligible compared to the shot noise, as the Josephson photonics device is operated at low temperature. Therefore, quantum fluctuations due to Cooper pair tunneling become dominant.

Conjecturing that one may still arrive at an effective Adler-like dynamical equation, there are obvious ways in which quantum effects will modify the picture of the phase particle in the washboard potential $U(\psi)$. The pointlike phase particle will be replaced by a wave function, where the scale of (zero-point) quantum fluctuations is associated with a mass assigned to the phase particle, which emerges from the scale of (single Cooper pair) charging effects. Classical thermal diffusion over the barrier is superseded by tunneling across the barrier between consecutive minima of $U(\psi)$ under the influence of dissipation. One may anticipate a particularly interesting regime in this competition between dissipation and tunneling, where the quantum dynamics of the phase particle is described by a Bloch-type wave function in the time crystal defined by potential $U(\psi)$, in spite of dissipative effects.

Setting up a full model of quantum dynamics of locking in the shot-noise dominated regime to study the quantum statistical properties of the microwave radiation emitted from the Josephson photonics, as well as deriving and studying resulting effective Adler-like equations are intriguing avenues for further research. It will link our investigations to interesting recent studies of locking for various systems, where the quantum character of the oscillator becomes crucial [39–46]. A further direction is uncovering parallels and distinctions between two different types of (quantum) phase slips; the tunneling of the phase of a dynamical solution, such as the Josephson phase in the injection locked devices studied here, and flux tunneling in thin superconducting wires [31].

V. HIGHER-ORDER RESONANCES

Part of the attraction of Josephson photonics devices is the variety of resonances associated with multiphoton creation, which are easily addressable in such devices by a simple change of the dc-voltage bias. In addition to the fundamental resonance at $2eV_{dc} \approx \hbar\omega_0$, there appear resonances at $2eV_{dc} \approx p\hbar\omega_0$ ($p \in \mathbb{N}$), whenever the bias provides each Cooper pair crossing the junction with the energy to excite p photons in the mode ω_0. Such processes were observed already in the very first experiment [5] and also play a pivotal role for the Josephson laser [3] where, however, they mix with fundamental ($p = 1$) resonances for higher modes $\omega_p = p\omega_0$ of the cavity. Equivalent processes in ac-driven Josephson devices [47] have very recently been observed for $p = 3$ down conversion [48–50].

In the classical description these processes, which based on a quantum picture may be called p-photon creation processes, materialize as (higher-order) parametric resonances in the equations of motion. Setting $R_0 \equiv 0$ and $\epsilon = 0$ for the
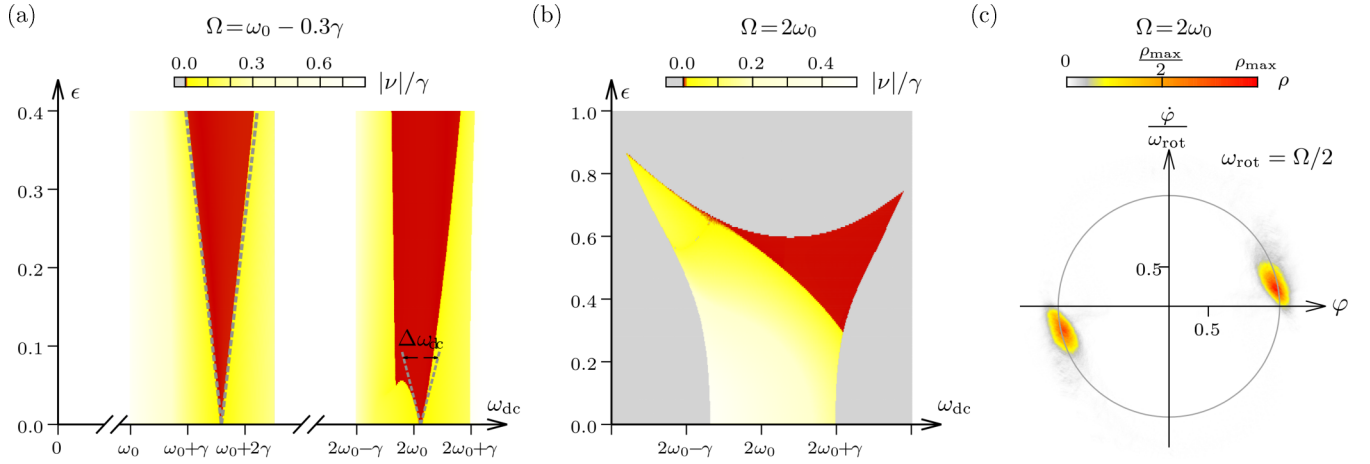
FIG. 6. (a) A locking signal with frequency $\Omega \approx \omega_0$ can lock a Josephson photonics system driven at different dc biases, $\omega_{dc} \approx p\Omega$, where each tunneling Cooper pair creates p photons with frequency ω_{dc}/p. The strongly nonlinear driving regime above the threshold of the ($p = 2$) parametric resonance, $\tilde{I}_c = 2.5 > 2 =: \tilde{I}_c^{thr}$, modifies the shape of the Arnold tongues. [Dashed lines show analytical results based on an extended theory (nonperturbative in $\tilde{I}_c$, see main text) for both $p = 1$ and $p = 2$. Parameters are $v_{R_0} = \omega_0/6$ and other parameters as in Fig. 1]. (b) The down-converted oscillations with frequency $\sim\omega_0$ at the ($p = 2$) parametric resonance can alternatively be locked by a signal oscillating at $\Omega \approx 2\omega_0$. The Arnold tongue [red, defined by $\nu(\epsilon) = [\omega_J(\epsilon) - \Omega]/2 \equiv 0$] appears at finite locking amplitude ϵ and crosses over into regions (gray), where directly driven oscillations at $\sim 2\omega_0$ prevail. (c) While a locking signal at $\Omega \approx \omega_0$ breaks the degeneracy of parametric oscillations, the degeneracy remains preserved for $\Omega = 2\omega_0$ as demonstrated by the phase-space distribution (in a frame rotating with $\Omega/2$) in the locked region ($\epsilon = 0.5$, $\omega_{dc} = 2\omega_0 + \gamma$). Noise ($S_\xi = 16\gamma/30$, $t_{corr} = 2/\gamma$) allows the system to slip between the two degenerate solutions, whose symmetry is not broken by the $\Omega = 2\omega_0$ locking signal.

moment, Eq. (1b), reduces to

$$\ddot{\varphi} + \gamma\dot{\varphi} + \omega_0^2\varphi = \tilde{I}_c\gamma\omega_0 \sin(\omega_{dc}t - \varphi)$$
$$\propto \frac{\varphi^{(p-1)}}{(p-1)!} \sin(\omega_{dc}t + \text{const.}). \quad (24)$$

The conventional parametric resonance occurs at $\omega_{dc} \approx 2\omega_0$, see Refs. [10–14,17,26] for details.

Important for our discussion below are two traits, which the conventional parametric ($p = 2$) and all higher-order ($p > 2$) resonances have in common: (i) Classically, there is a driving threshold above which a solution $\tilde{\varphi}(\omega = \omega_{dc}/p) = 0$ becomes unstable and a parametric oscillation emerges. (ii) The parametric solution with period $T^{(p)} = \frac{2\pi}{\omega_{dc}/p} = pT^{drive}$ is p-fold degenerate, with the p solutions connected through time translation by an integer multiple of the period of the (effective) parametric drive $T^{drive} := 2\pi/\omega_{dc}$. This corresponds to a p-fold symmetry in phase space [with solutions $\tilde{\varphi}_k(\omega_{dc}/p) = e^{i2\pi k/p} \tilde{\varphi}_{k=0}(\omega_{dc}/p)$ with $k = 0 \ldots p - 1$]. The p-fold symmetry has been described in the language of a spontaneous breaking of a discrete symmetry and termed phase-space time crystal [51–55].

The physics of phase locking at higher-order resonances is very rich and considerably more complex compared to the fundamental resonance; for one, due to the fact that the unlocked (classical) solution only exists in a nonlinear regime. Here, we do not want to discuss locking at higher-order resonances at the same level of detail as done for the fundamental resonance above. Instead, we only briefly present first results for $p = 2$. These are chosen to highlight a specific locking feature, newly arising for the $p > 1$ case, which is of both fundamental interest and practical relevance for possible applications (e.g., for stabilizing a squeezing axis). The locking

signal aimed at stabilizing the phase and frequency of the oscillations at the (down-converted) slow frequency, ω_{dc}/p, can either *break, or preserve* the discrete p-fold time-translation symmetry. The symmetry will be broken by providing a signal at the slow frequency, $\Omega \sim \omega_{dc}/p \simeq \omega_0$, but preserved by providing a signal at the fast frequency, $\Omega \simeq \omega_{dc} \simeq p\omega_0$.

In the first case, the very same locking signal at $\Omega \simeq \omega_0$ can actually lock a Josephson photonics system driven at (two or even multiple) different dc biases; namely around the fundamental resonance, $\omega_{dc} \simeq \omega_0$, but also around the higher-order resonances, $\omega_{dc} \simeq p\omega_0$. This is demonstrated in Fig. 6(a), which shows the Arnold tongues of locked cavity oscillations with frequency Ω for fixed locking signal frequency $\Omega \simeq \omega_0$ and varying dc bias and locking amplitude. Shown are results from the numerical solutions of the full equations of motion, Eqs. (1), for a driving strength above the threshold of ($p = 2$) parametric oscillations, compared to analytical results for the locking region's boundaries, based on Adler-like equations for slow variables. For the parametric case, we can make an ansatz analogous to Eqs. (6) and (7), and expand around the $\epsilon = 0$ solutions determined by nonlinear equations involving Bessel functions [11,12,17]. We find a locking region with width $\Delta\omega_{dc}$ [as in Fig. 6(a)] that scales similarly to the fundamental resonance case as $\Delta\omega_{dc} = Av_{R_0}$ with a numerical prefactor $A \approx 1.41$ for the parameters of Fig. 6(a). [The numerical value of A depends on the nonlinear solutions of equations containing various Bessel functions in an involved manner, but we find $A \sim O(1)$ away from bifurcations of the equations.] Dashed lines in Fig. 6(a) also shows analytical results for the width of the Arnold tongue for $p = 1$ obtained by extending Eqs. (8)–(9b) for larger driving $\tilde{I}_c$ and expanding in ϵ the resulting Bessel-function expressions. For this case $p = 1$, the width of the Arnold tongue is given by $\Delta\omega_{dc} = B\epsilon v_{R_0}$ where

$B \approx 0.626$ for the parameters of Fig. 6(a). Clearly, the mixing of down-converted and direct drive, and the nonlinearity of the $\epsilon = 0$ solution limits the validity of this ansatz more severely for $p \geqslant 2$ than for the $p = 1$ case, and capturing all features of Fig. 6(a) is beyond its scope.

For the second case, where the locking signal is provided at the fast frequency, $\Omega \approx \omega_{\mathrm{dc}} \approx 2\omega_0$, Fig. 6(b) reveals that a large locking amplitude is required even for optimal detuning, i.e., the Arnold tongue does not touch the $\epsilon = 0$ axis. Intuitively one may argue, that to lock oscillations at the slow frequency, $\Omega/p \sim \omega_0$, a locking signal provided at the fast frequency, $\Omega \sim \omega_{\mathrm{dc}} \sim p\omega_0$, has to be down converted, which only becomes effective above a certain threshold of signal strength ϵ. Moreover, however, there will be competition between direct locking of the cavity oscillations to a frequency Ω and the desired parametric locking to Ω/p. The extended Adler-like effective description of parametric locking that could explain the details of Fig. 6(b) remains a subject for further studies. What is known and strikingly demonstrated by Fig. 6(c) is the crucial coveted feature of parametric locking: the preservation of the p-fold phase-space symmetry. As can be seen directly from the equations of motion, if a solution, where the cavity is locked at the slow frequency, Ω/p, exists, it is degenerate and there exist p-equivalent solutions for the cavity oscillations shifted by an integer multiple of $2\pi/\Omega$ in time, or rotated by an integer multiple of $2\pi/p$ in phase space. In the phase-space distribution of Fig. 6(c) the twofold symmetry is clearly seen. In presence of noise as discussed in Sec. IV, the cavity oscillations will explore both possible degenerate solutions.

We expect that the scenario of the parametric locking that preserves symmetry will also be reproduced in a quantum description. This mechanism may be used, for instance, to reduce the diffusion of the orientation of the squeezing axis for degenerate or nondegenerate emission of quantum microwave radiation from dc-biased Josephson photonics devices without modifying other desired quantum emission properties. It may also considerably simplify experiments such as the recent confirmation of entanglement in Ref. [9] and enable new applications. Note, that a recent experiment on nondegenerate parametric oscillations [49] follows the diametrically opposite approach of applying a weak on-resonant tone as described above and consequently breaks the phase-space symmetry.

VI. SYNCHRONIZATION

The phenomenon of synchronization describes the mutual phase locking of weakly coupled self-sustained oscillators [34,56,57]. We envision a situation where two Josephson devices, each modeled by a circuit such as studied in the previous sections, are weakly coupled. Experimentally a capacitive, inductive or even resistive coupling can be easily realized and potentially tunable (or nonlinear) coupling scenarios could also be engineered by linking the two devices by a Josephson junction or more complex circuit.

The universal nature of synchronization implies that the resulting mutually locked dynamics are qualitatively similar for any of these type of couplings between the devices (even though variations may be envisioned for time-delayed or strongly nonlinear couplings). To provide an example of
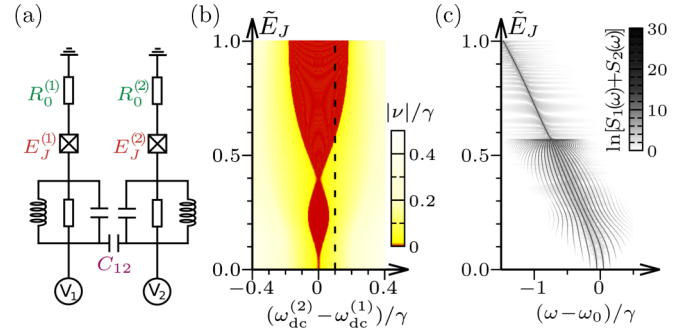

FIG. 7. Synchronization of Josephson oscillators. (a) Sketch of two lockable Josephson photonics circuits, which can synchronize if weakly coupled (e.g., by a capacitance). (b) Arnold tongue indicating the voltage detuning between the two circuits, where oscillations synchronize [red, $\nu(\epsilon) = (\omega_J^{(2)} - \omega_J^{(1)})/\gamma$], as the effective coupling increases with $\tilde{E}_J$. The coupling terms in the Adler-Kuramoto equations (29) scale with the critical detuning parameters (30), $\nu_c^{(\sigma)} \propto (\tilde{E}_J)^2$, explaining the shape of the tongue for weak coupling, while the change of Josephson frequencies with $\tilde{E}_J$ yields more complex behavior [such as multiple (de)synchronization transitions] at larger $\tilde{E}_J$. [results for identical cavities ($\tilde{E}_J^{(1)} = \tilde{E}_J^{(2)} = \tilde{E}_J$, etc.) with antisymmetric bias, $\omega_{\mathrm{dc}}^{(2/1)} = \omega_0 \pm (\omega_{\mathrm{dc}}^{(2)} - \omega_{\mathrm{dc}}^{(1)})$ and parameters as in Fig. 1; $\epsilon^{(\sigma)} = C_{12}/(C^{(\sigma)} + C_{12}) = 0.01$.] (c) (Sum) spectrum at bias $\omega_{dc}^{(2/1)} = \omega_0 \pm \gamma/20$ [dashed in (b)] showing frequency pulling and a fan of frequencies before both cavities synchronize to emit with a common single frequency for large $\tilde{E}_J$.

the dynamics, we have chosen to describe two Josephson circuits coupled by a mutual capacitance C_{12}, as depicted in Fig. 7, assumed small compared to the capacitance of the circuits $C_{12} \ll C^{(1)}, C^{(2)}$. We will demonstrate that the capacitive coupling leads to synchronization of the Josephson photonics devices. However, the formalism presented, as well as the qualitative aspects of our discussion, apply to any coupling mechanism.

The system in Fig. 7 is governed by the following (Kirchhoff) equations of motion

$$\dot{\varphi}_J^{(\sigma)} = \omega_{\mathrm{dc}}^{(\sigma)} - v_{R_0}^{(\sigma)} \sin\left(\varphi_J^{(\sigma)}\right) - \dot{\varphi}^{(\sigma)} \qquad (25\mathrm{a})$$

$$Z^{(\sigma)}\left[\varphi^{(\sigma)}\right] = \tilde{I}_c^{(\sigma)} \sin\left(\varphi_J^{(\sigma)}\right) + \frac{\epsilon^{(\sigma)}}{\omega_0^{(\sigma)} \gamma^{(\sigma)}} \ddot{\varphi}^{(\bar{\sigma})} \qquad (25\mathrm{b})$$

where we have introduced superscripts $\sigma = 1, 2$ to label the two devices and $\bar{\sigma}$, defined as $\bar{\sigma} = 2$ if $\sigma = 1$, $\bar{\sigma} = 1$ if $\sigma = 2$.

The dimensionless response $Z^{(\sigma)}$ that describes the two cavities is defined by

$$Z^{(\sigma)}\left[\varphi^{(\sigma)}\right] = \frac{1}{\omega_0^{(\sigma)} \gamma^{(\sigma)}}\left[\ddot{\varphi}^{(\sigma)} + \gamma^{(\sigma)} \dot{\varphi}^{(\sigma)} + \left(\omega_0^{(\sigma)}\right)^2 \varphi^{(\sigma)}\right],$$

$$(26)$$

and further notation is summarized in Table II.

In close analogy to our calculations for locking in Sec. III we can now derive an effective equation for the slow dynamics describing how and in which parameter region the two systems synchronize. The synchronization region corresponds to a range of detuning values between the two dc voltages, $\omega_{\mathrm{dc}}^{(2)} - \omega_{\mathrm{dc}}^{(1)}$, where due to the coupling ϵ the frequency of Josephson oscillations will be identical in both circuits. To derive the

TABLE II. Physical quantities that characterize the two devices, $\sigma = 1, 2$.

Physical quantity	Parametrization	Unit
resonance frequencies	$\omega_0^{(\sigma)}$	s^{-1}
resonance widths	$\gamma^{(\sigma)} = (R^{(\sigma)}C^{(\sigma)})^{-1}$	s^{-1}
dc bias voltages	$\omega_{dc}^{(\sigma)} = (2e/\hbar)V^{(\sigma)}$	s^{-1}
Josephson frequencies	$\omega_J^{(\sigma)} \neq \omega_{dc}^{(\sigma)}$	s^{-1}
scale of residual voltages	$v_{R_0}^{(\sigma)} = (2e/\hbar)I_c^{(\sigma)}R_0^{(\sigma)}$	s^{-1}
Josephson driving strengths	$\tilde{I}_c^{(\sigma)} = (2e/\hbar)I_c^{(\sigma)}R^{(\sigma)}/\omega_0^{(\sigma)}$	1
coupling strengths	$\epsilon^{(\sigma)} = C_{12}/(C^{(\sigma)} + C_{12})$	1

Kuramoto-Adler equations, from which the boundaries of the synchronization region follow, we introduce slowly varying functions, as in Sec. III, for the Josephson and cavity phases,

$$\varphi_J^{(\sigma)} = \omega_J^{(\sigma)} + \theta_J^{(\sigma)}(t) + a^{(\sigma)} \sin\left[\omega_J^{(\sigma)}t + \phi_J^{(\sigma)}(t)\right], \quad (27)$$

$$\varphi^{(\sigma)} = b^{(\sigma)} \sin\left[\omega_J^{(\sigma)}t + \phi^{(\sigma)}(t)\right]. \quad (28)$$

The ansatz above is consistent with the limit of weak driving $\tilde{I}_c^{(\sigma)} \ll 1$ and small low-frequency impedance $R_0^{(\sigma)} \ll R^{(\sigma)}$. Assuming time-scale separation and further approximations (see Supplemental Material [37] for details) a system of coupled equations for the slowly varying functions can be derived, which finally reduces for weak capacitative coupling to the Kuramoto model

$$\dot{\theta}_J^{(1)} = \tilde{v}^{(1)} + \epsilon_1 v_c^{(1)} \sin[\nu_J t + \theta_J^{(2)} - \theta_J^{(1)} - \chi^{(1)} - \chi^{(2)}] \quad (29a)$$

$$\dot{\theta}_J^{(2)} = \tilde{v}^{(2)} - \epsilon_2 v_c^{(2)} \sin[\nu_J t + \theta_J^{(2)} - \theta_J^{(1)} + \chi^{(1)} + \chi^{(2)}]. \quad (29b)$$

Here, $\tilde{v}^{(\sigma)} \equiv \omega_J^{(\sigma)}(\epsilon = 0) - \omega_J^{(\sigma)}$ denotes the detuning between the Josephson frequency in absence of coupling, $\omega_J^{(\sigma)}(\epsilon = 0)$, i.e., at $C_{12} = 0$, and the Josephson frequency ω_J affected by mutual frequency pulling. The two critical detuning parameters ν_c^i are found to be

$$v_c^{(1)} = \frac{1}{2} v_{R_0}^{(1)} \frac{\omega_J^{(1)}}{\gamma^{(2)}} \frac{\tilde{I}_c^{(2)}}{|z^{(1)}||z^{(2)}|}, \quad (30a)$$

$$v_c^{(2)} = \frac{1}{2} v_{R_0}^{(2)} \frac{\omega_J^{(2)}}{\gamma^{(1)}} \frac{\tilde{I}_c^{(1)}}{|z^{(1)}||z^{(2)}|}. \quad (30b)$$

Both set of parameters depend on complex dimensionless impedances $z^{(\sigma)} \equiv |z^{(\sigma)}|e^{i\chi^{(\sigma)}} = (2v^{(\sigma)} + i\gamma^{(\sigma)})/\gamma^{(\sigma)}$, that are obtained from the Fourier transform of the responses $Z^{(\sigma)}$ evaluated at the detuning between the corresponding Josephson frequency and the resonance (see Supplemental Material [37]). This forms an implicit set of equations together with the definition of the Josephson frequency [based on averaging Eq. (25a)]

$$\omega_J^{(\sigma)} = \omega_{dc}^{(\sigma)} - \frac{1}{2} \frac{(v_{R_0}^{(\sigma)})^2}{\omega_0^{(\sigma)}} + \frac{1}{2} \frac{\tilde{I}_c^{(\sigma)}}{|z^{(\sigma)}|} v_{R_0}^{(\sigma)} \sin(\chi^{(\sigma)}). \quad (31)$$

Notably, the Josephson frequency without coupling $\omega_J^{(\sigma)}(\epsilon = 0)$ depends only on the parameters of the corresponding device $\sigma = 1, 2$.

Of particular interest in Eq. (29) is the appearance of the phases $\chi^{(\sigma)}$ of the oscillators' impedances. These reflect the indirect nature of the coupling of the synchronized Josephson-junction phases. Building on the notion that synchronization can be understood as one junction locking onto a signal provided by the other junction's oscillation, we can immediately discern from Fig. 7(a) that the locking signal is mediated by the cavities. The signal provided by the first Josephson junction's oscillation driving its cavity thus comes with an extra phase $\chi^{(1)}$ determined by that cavity's response function. That signal, in turn, drives the second circuit via an oscillating current, i.e., in a manner slightly different from the oscillating voltage drive considered in Secs. II and III. Considering the corresponding changes to the circuit equations (1) and the resulting Eqs. (8)–(9b), one notes that the cavity response enters again and brings an extra phase of $\chi^{(2)}$, thus explaining the phase shifts in Eq. (29). Also interesting to note considering Eq. (29) is the fact that the effective coupling can be amplified by a dimensionless factor, $\omega_J^{(\sigma)}/\gamma^{(\bar{\sigma})}$, similar to the quality factors of the cavities. Therefore, a significant coupling can be achieved between high quality factor Josephson devices despite a relatively low value of the mutual capacitance.

To emphasize the connection to an Adler-type equation, we define the relative phase of the Josephson oscillations $\psi \equiv \tilde{\varphi}_J^{(2)} - \tilde{\varphi}_J^{(1)} = \nu_J t + \theta_J^{(2)} - \theta_J^{(1)}$, where we introduced slow Josephson phases $\tilde{\varphi}_J^{(\sigma)} = \omega_J^{(\sigma)}t + \theta_J^{(\sigma)}$, obtained from the total Josephson phase, Eq. (27), by averaging over time scales of the order of $2\pi/\omega_J^{(\sigma)}$. With this definition, the condition of synchronization corresponds to $\dot{\psi} = 0$. The difference of the two Adler-Kuramoto equations yields an Adler-type equation for $\psi(t)$,

$$\dot{\psi} = \tilde{v}^{(2)} - \tilde{v}^{(1)} - v_{eff} \sin(\psi + \chi_{eff}), \quad (32)$$

with the effective critical detuning v_{eff} and effective phase offset χ_{eff} given by

$$v_{eff} = \sqrt{\left(\epsilon^{(1)}v_c^{(1)}\right)^2 + \left(\epsilon^{(2)}v_c^{(2)}\right)^2};$$

$$\chi_{eff} = \arctan\left[\frac{\epsilon^{(2)}v_c^{(2)} - \epsilon^{(1)}v_c^{(1)}}{\epsilon^{(1)}v_c^{(1)} + \epsilon^{(2)}v_c^{(2)}} \tan\left(\chi^{(1)} + \chi^{(2)}\right)\right]. \quad (33)$$

Figure 7(b) illustrates the Arnold tongue described by the effective Adler equation, Eq. (32), where we ramp up the effective coupling by increasing the Josephson driving strengths, assumed equal for the two devices. The possibility to achieve synchronization by tuning the Josephson driving strength (using SQUIDs) may be experimentally more immediately feasible than direct control of the coupling capacitance. At low coupling, the synchronization window increases proportional to the square of the Josephson driving strength, $v_{eff} \propto \tilde{I}_c^2$, consistent with the behavior predicted by Eq. (30). Remarkably, the synchronization window is not increasing monotonously with the Josephson driving strength, suggesting the experiment may exhibit sweet spots where synchronization is more efficient. Examining the analytical expressions, the behavior can be attributed to the dependence of the effective coupling on the dimensionless impedances z_1 and z_2 of the two coupled cavities. Due to frequency pulling, the detunings $v^{(\sigma)}$ may pass through their corresponding res-

onance ($\nu^{(\sigma)} = 0$) at different values of the Josephson driving strength, giving rise to a complicated dependence of the effective coupling.

VII. CONCLUSIONS

In this paper, we have studied injection locking and synchronization in Josephson photonics devices in the classical regime. We found that a residual resistance in series to the Josephson junction-cavity circuit is a crucial ingredient. If it is accounted for, a single-mode circuit weakly driven at its fundamental resonance undergoes self-sustained oscillations and therefore constitutes the simplest Josephson photonics device that can be injection locked and synchronized.

Based on the fundamental Kirchhoff circuit equations we derived an Adler-type equation describing locking to an additional ac voltage by a time-scale separation ansatz. The predicted scaling of the locking region with the device parameters will allow experimentalists to devise optimal circuit designs. Bounds on electrical noises against which the phase of cavity oscillations can be stabilized were derived and the noise dependence of the (strongly reduced) linewidth of the cavity emission were discussed.

At a parametric dc-voltage drive $\omega_{\text{dc}} \approx 2\omega_0$, the down-converted oscillations can be locked with an ac signal being either at the parametric driving frequency, $\Omega \approx \omega_{\text{dc}}$, or at the down-converted frequency, $\Omega \approx \omega_{\text{dc}}/2$. These two scenarios correspond to breaking and preserving of the twofold time-translation symmetry of the cavity oscillations. In the latter case, noise allows for slips between the two degenerate solutions, yielding a phase-space distribution with two metastable solutions in the locked steady state. The phase stabilization of Josephson photonics devices by locking will boost their potential as sources of entangled and squeezed quantum microwaves.

Finally, we extended the model to study synchronization between two Josephson photonics devices. An analytical derivation of a Kuramoto-Adler-type equation again allows quantitative statements on the parameter dependence of synchronization regions, identified by characteristic emission spectra and easily mapped out by tuning the Josephson energy of the two devices.

While in this work the dynamics of the Josephson photonics circuits is governed by classical circuit equations and we studied stability against classical noise, the generic features of the locking and synchronization mechanism, in particular, the importance of an in-series resistance, are expected to carry over to a considerable extent to current experimental devices. These can be designed or tuned to operate in regimes where the dynamics are more or less strongly affected by quantum fluctuations, so that Josephson photonics devices may allow for a systematic study of locking and synchronization from the semiclassical to the deep quantum regime. A full theoretical quantum mechanical description including the residual resistance will be required to properly describe regimes where shot noise becomes more dominant than thermal voltage noise and to study such fascinating problems as quantum slips of the phase of the emitted light.

[1] Y.-Y. Liu, J. Stehlik, C. Eichler, M. J. Gullans, J. M. Taylor, and J. R. Petta, Science **347**, 285 (2015).

[2] D. Marković, J. D. Pillet, E. Flurin, N. Roch, and B. Huard, Phys. Rev. Appl. **12**, 024034 (2019).

[3] M. C. Cassidy, A. Bruno, S. Rubbert, M. Irfan, J. Kammhuber, R. N. Schouten, A. R. Akhmerov, and L. P. Kouwenhoven, Science **355**, 939 (2017).

[4] F. Chen, J. Li, A. D. Armour, E. Brahimi, J. Stettenheim, A. J. Sirois, R. W. Simmonds, M. P. Blencowe, and A. J. Rimberg, Phys. Rev. B **90**, 020506(R) (2014).

[5] M. Hofheinz, F. Portier, Q. Baudouin, P. Joyez, D. Vion, P. Bertet, P. Roche, and D. Estève, Phys. Rev. Lett. **106**, 217005 (2011).

[6] A. Grimm, F. Blanchet, R. Albert, J. Leppäkangas, S. Jebari, D. Hazra, F. Gustavo, J.-L. Thomassin, E. Dupont-Ferrier, F. Portier, and M. Hofheinz, Phys. Rev. X **9**, 021016 (2019).

[7] C. Rolland, A. Peugeot, S. Dambach, M. Westig, B. Kubala, Y. Mukharsky, C. Altimiras, H. le Sueur, P. Joyez, D. Vion, P. Roche, D. Esteve, J. Ankerhold, and F. Portier, Phys. Rev. Lett. **122**, 186804 (2019).

[8] M. Westig, B. Kubala, O. Parlavecchio, Y. Mukharsky, C. Altimiras, P. Joyez, D. Vion, P. Roche, D. Esteve, M. Hofheinz,

M. Trif, P. Simon, J. Ankerhold, and F. Portier, Phys. Rev. Lett. **119**, 137001 (2017).

[9] A. Peugeot, G. Ménard, S. Dambach, M. Westig, B. Kubala, Y. Mukharsky, C. Altimiras, P. Joyez, D. Vion, P. Roche, D. Esteve, P. Milman, J. Leppäkangas, G. Johansson, M. Hofheinz, J. Ankerhold, and F. Portier, Phys. Rev. X **11**, 031008 (2021).

[10] C. Padurariu, F. Hassler, and Y. V. Nazarov, Phys. Rev. B **86**, 054514 (2012).

[11] V. Gramich, B. Kubala, S. Rohrer, and J. Ankerhold, Phys. Rev. Lett. **111**, 247002 (2013).

[12] A. D. Armour, M. P. Blencowe, E. Brahimi, and A. J. Rimberg, Phys. Rev. Lett. **111**, 247001 (2013).

[13] J. Leppäkangas, G. Johansson, M. Marthaler, and M. Fogelström, Phys. Rev. Lett. **110**, 267004 (2013).

[14] B. Kubala, V. Gramich, and J. Ankerhold, Phys. Scr. **T165**, 014029 (2015).

[15] A. D. Armour, B. Kubala, and J. Ankerhold, Phys. Rev. B **91**, 184508 (2015).

[16] M. Trif and P. Simon, Phys. Rev. B **92**, 014503 (2015).

[17] S. Meister, M. Mecklenburg, V. Gramich, J. T. Stockburger, J. Ankerhold, and B. Kubala, Phys. Rev. B **92**, 174532 (2015).

[18] J.-R. Souquet and A. A. Clerk, Phys. Rev. A **93**, 060301(R) (2016).

[19] J. Leppäkangas, M. Fogelström, M. Marthaler, and G. Johansson, Phys. Rev. B **93**, 014506 (2016).

[20] A. D. Armour, B. Kubala, and J. Ankerhold, Phys. Rev. B **96**, 214509 (2017).

[21] H. Wang, M. P. Blencowe, A. D. Armour, and A. J. Rimberg, Phys. Rev. B **96**, 104503 (2017).

[22] S. H. Simon and N. R. Cooper, Phys. Rev. Lett. **121**, 027004 (2018).

[23] J. Leppäkangas, M. Marthaler, D. Hazra, S. Jebari, R. Albert, F. Blanchet, G. Johansson, and M. Hofheinz, Phys. Rev. A **97**, 013855 (2018).

[24] L. Arndt and F. Hassler, Phys. Rev. B **100**, 014505 (2019).

[25] W. T. Morley, A. Di Marco, M. Mantovani, P. Stadler, W. Belzig, G. Rastelli, and A. D. Armour, Phys. Rev. B **100**, 054515 (2019).

[26] B. Kubala, J. Ankerhold, and A. D. Armour, New J. Phys. **22**, 023010 (2020).

[27] B. Lang and A. D. Armour, New J. Phys. **23**, 033021 (2021).

[28] A. M. Hriscu and Y. V. Nazarov, Phys. Rev. Lett. **110**, 097002 (2013).

[29] A. Bezryadin, C. N. Lau, and M. Tinkham, Nature (London) **404**, 971 (2000).

[30] F. Altomare, A. M. Chang, M. R. Melloch, Y. Hong, and C. W. Tu, Phys. Rev. Lett. **97**, 017001 (2006).

[31] O. V. Astafiev, L. B. Ioffe, S. Kafanov, Y. A. Pashkin, K. Y. Arutyunov, D. Shahar, O. Cohen, and J. S. Tsai, Nature (London) **484**, 355 (2012).

[32] Y. Chen, Y.-H. Lin, S. D. Snyder, A. M. Goldman, and A. Kamenev, Nature Phys. **10**, 567 (2014).

[33] R. Adler, Proc. IRE **34**, 351 (1946).

[34] A. Pikovsky, M. G. Rosenblum, and J. Kurths, *Synchronization, A Universal Concept in Nonlinear Sciences* (Cambridge University Press, Cambridge, 2001).

[35] S. Shapiro, Phys. Rev. Lett. **11**, 80 (1963).

[36] C. A. Hamilton, Rev. Sci. Instrum. **71**, 3611 (2000).

[37] See Supplemental Material at http://link.aps.org/supplemental/10.1103/PhysRevB.104.054517 for details on locking by direct ac-current injection into the cavity, for the derivation of the effective Kuramoto equations, and for notes on the numerical calculations.

[38] H. A. Kramers, Physica **7**, 284 (1940).

[39] S. Walter, A. Nunnenkamp, and C. Bruder, Phys. Rev. Lett. **112**, 094102 (2014).

[40] N. Lörch, E. Amitai, A. Nunnenkamp, and C. Bruder, Phys. Rev. Lett. **117**, 073601 (2016).

[41] N. Lörch, S. E. Nigg, A. Nunnenkamp, R. P. Tiwari, and C. Bruder, Phys. Rev. Lett. **118**, 243602 (2017).

[42] A. Roulet and C. Bruder, Phys. Rev. Lett. **121**, 053601 (2018).

[43] E. Amitai, M. Koppenhöfer, N. Lörch, and C. Bruder, Phys. Rev. E **97**, 052203 (2018).

[44] M. Koppenhöfer and A. Roulet, Phys. Rev. A **99**, 043804 (2019).

[45] M. R. Jessop, W. Li, and A. D. Armour, Phys. Rev. Res. **2**, 013233 (2020).

[46] L. Ben Arosh, M. C. Cross, and R. Lifshitz, Phys. Rev. Res. **3**, 013130 (2021).

[47] W. Wustmann and V. Shumeiko, Low Temp. Phys. **45**, 848 (2019).

[48] I.-M. Svensson, A. Bengtsson, P. Krantz, J. Bylander, V. Shumeiko, and P. Delsing, Phys. Rev. B **96**, 174503 (2017).

[49] I.-M. Svensson, A. Bengtsson, J. Bylander, V. Shumeiko, and P. Delsing, Appl. Phys. Lett. **113**, 022602 (2018).

[50] C. W. Sandbo Chang, C. Sabín, P. Forn-Díaz, F. Quijandría, A. M. Vadiraj, I. Nsanzineza, G. Johansson, and C. M. Wilson, Phys. Rev. X **10**, 011011 (2020).

[51] L. Guo, M. Marthaler, and G. Schön, Phys. Rev. Lett. **111**, 205303 (2013).

[52] Y. Zhang, J. Gosner, S. M. Girvin, J. Ankerhold, and M. I. Dykman, Phys. Rev. A **96**, 052124 (2017).

[53] J. Gosner, B. Kubala, and J. Ankerhold, Phys. Rev. B **101**, 054501 (2020).

[54] P. Liang, M. Marthaler, and L. Guo, New J. Phys. **20**, 023043 (2018).

[55] F. Nathan, G. Refael, M. S. Rudner, and I. Martin, Phys. Rev. Res. **2**, 043411 (2020).

[56] Y. Kuramoto, Lect. Notes Phys. **30**, 420 (1975).

[57] J. A. Acebrón, L. L. Bonilla, C. J. Pérez Vicente, F. Ritort, and R. Spigler, Rev. Mod. Phys. **77**, 137 (2005).